12-1-2017

Confined Photonic Mode Propagation Observed in Photoemission Electron Microscopy

Theodore Stenmark
Portland State University

Robert Campbell Word
Portland State University, wordr@pdx.edu

Rolf Konenkamp
Portland State University, rkoe@pdx.edu

Citation Details

Published as: Stenmark, T., Word, R. C., & Könenkamp, R. (2017). Confined photonic mode propagation observed in photoemission electron microscopy. Ultramicroscopy, 183, 38-42.

Confined Photonic Mode Propagation Observed in Photoemission Electron Microscopy

Theodore Stenmark, R. C. Word, R. Könenkamp
Department of Physics, Portland State University, Portland, Oregon, 97207

Abstract

Using photoemission electron microscopy (PEEM) we present a comparative analysis of the wavelength dependence of propagating fields in a simple optical slab waveguide and a thin film photonic crystal W1-type waveguide. We utilize an interferometric imaging approach for light in the near-ultraviolet regime where a 2-photon process is required to produce photoelectron emission. The typical spatial resolution in these experiments is <30nm. Electromagnetic theory and finite element simulations are shown to be in good agreement with the experimental observations. Our results indicate that multiphoton PEEM is a useful sub-wavelength characterization technique in thin film optics.

1. Introduction

Photoemission Electron Microscopy (PEEM) is an imaging technique where photo-emitted electrons are collected from a sample surface and used to form images with spatial resolution down to 5nm [1]. Continuous or pulsed x-ray, ultraviolet, visible and infrared light have been used in the past to generate the photoelectrons. Contrast depends on the spatial electron yield of the photo-emitted electrons, which in turn depends on the work function, surface electron density, surface topography, as well as intensity and energy of the incident photons. The dependence on photon and electron density makes PEEM a powerful technique for observation of electromagnetic near-field phenomena. In multiphoton PEEM the photoemission process involves multiple photons for a single electron emission and allows the visualization of visible light fields at sample surfaces with high contrast and sub-wavelength resolution. When pulsed excitation light is used, time-resolved observation down to sub-femtosecond timescales is possible [2].

In recent years, multi-photon PEEM has been used extensively for the study of surface plasmon polaritons [3, 4] whose ability to confine light past the diffraction limit has attracted considerable attention. Less explored is the potential of multi-photon PEEM to probe the electromagnetic fields at the surface of photonic dielectric materials and devices. In the past years we have characterized thin film wave-guiding structures with this technique [5, 6]. Using a pulsed laser source we create a standing interference pattern between the confined modes of the waveguide structure and the incident illumination. From this pattern we are able to characterize the energy propagation in photonic devices in considerable detail [7].

In this paper we discuss two experimental situations in thin optical waveguides demonstrating the advantages of the very high spatial resolution available in aberration-corrected PEEM and the analytical power of interferometric imaging. First we determine the wavelength dependence of modes in a planar slab waveguide. Second we look beyond the slab waveguide and turn to the modes in a line defect within a photonic crystal structure to determine the dependence of the effective index on wavelength.

2. Experimental methods

The sample consisted of a 0.2mm borosilicate glass slide covered with a 290nm ± 20nm thick indium-tin-oxide (ITO) layer. In this configuration the ITO layer is bounded by two media of lower refractive index, glass and air, and hence forms a slab waveguide. A narrow trench was milled through the ITO layer with an FEI strata 273 focused ion beam (FIB) to allow light to couple into the ITO layer via diffraction. A hexagonal photonic crystal (PC) lattice structure was milled into the ITO/borosilicate sample with a periodicity of 180nm and an approximate hole diameter of 90nm. Oriented perpendicular to the coupling trench the photonic crystal structure had a single row of missing hole forming un-milled region of ITO as seen in Fig. 1a. This creates a W1-type line defect waveguide. As seen from the figure there are also un-milled regions outside the photonic crystal area. These are used as simple slab waveguides to set up a direct comparison to the defect waveguide with in the PC.

The sample illumination in the PEEM was provided by a Spectra-Physics Mai Tai TI:Sapphire laser with 60fs pulse duration at a repetition rate of 100MHz and a Del Mar second harmonic generator to up-convert the fundamental infrared pulses to wavelengths covering the interval 390nm < λ <415nm. The sample was oriented in the microscope such that the laser illumination was incident perpendicular to the coupling trench and at an incident angle of 60˚ from the sample surface normal as seen in Fig. 1b. Images were taken over a range of wavelengths from 415nm to 390nm with transverse electric (TE) polarization. ITO has a work function of 4.2eV [8] which requires a 2-photon process for photoemission at these photon energies.

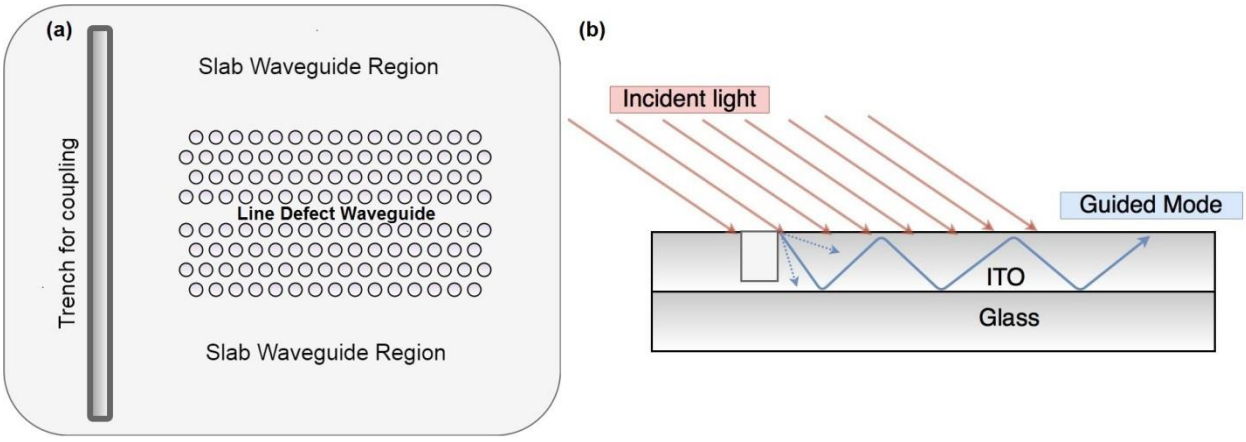

Fig. 1. (a) Schematic showing a top down view of the sample. (b) Side view demonstrating the coupling of incident light into the ITO layer. Incident light diffracts off the edge of the trench into the ITO layer where the waveguide selects for allowed modes. The guided modes interfere with the incident light to create a stationary interference pattern.

3. Simulation

Simulations were conducted in COMSOL Multiphysics, an iterative finite element program. For the slab waveguide there is symmetry in the plane perpendicular to the ITO layer, which allows for a 2D simulation of the system. The same symmetry is not afforded for the photonic crystal defect waveguide, so a full 3D treatment is necessary. An electromagnetic field is defined incident on an ITO layer with a coupling trench as seen in Figs. 2a and c. Since the electrons

collected in PEEM come from the near-surface region of the sample, the time averaged field at the surface of the ITO is responsible for the observed interference pattern as depicted in Figs. 2b and d, and is taken as the starting point of the physical interpretation.

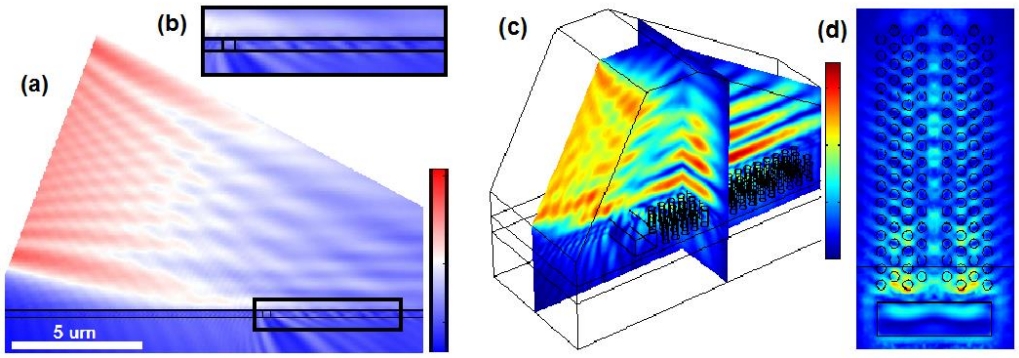

Fig. 2. (a) Overview for a 2D simulation of the cross section slab waveguide showing $|E|^2$. (b) Close up of the cross section of the ITO guiding region. (c) Overview for a 3D simulation of the photonic crystal waveguide. (d) $|E|^2$ at the cross section at the ITO-vacuum interface of the photonic crystal.

4. Experimental results and analysis

In Figure 3a we show a standard PEEM image obtained with continuous wave 244nm ultraviolet illumination to present an overview of the sample geometry and the topography in the area of interest. The image uses single-photon excitation and shows interference and diffraction effects only very weakly. Figure 3b is taken with photon energies of ~3eV (λ~400nm) in femtosecond pulses. The image is primarily formed using non-linear 2-photon processes and light-optical interference and diffraction effects are enhanced in the presentation. The interference pattern seen on the surface of the sample is created by light propagating in the ITO layer and the incident laser beam approaching the sample surface through vacuum. The photoelectron yield is proportional to the electric field to the 2n power [5],

$$YPE \propto ||E_{tot}||^{2n}, \quad (1)$$

where n is the number of photons required to excite a single electron emission, i.e. here n=2. The nonlinearity of the multiphoton process enhances contrast between areas of constructive and destructive interference as seen in Fig. 3b.

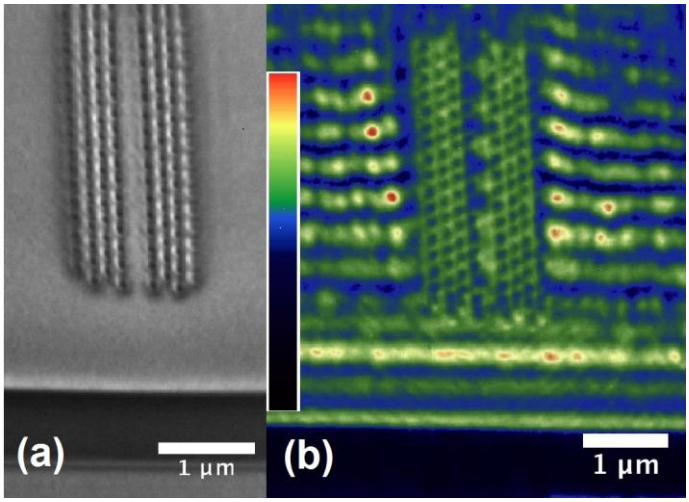

Fig. 3. (a) PEEM images of the photonic crystal defect waveguide with ultraviolet illumination, requiring a single photon excitation process. (b) Colorized image of defect waveguide and slab waveguide with 410nm pulsed illumination requiring a 2-photon process for the photoemission.

We analyzed the interference patterns in the planar slab regions and in the PC waveguide by determining the laterally averaged pixel intensity along the propagation direction in the waveguides. The resulting line graphs are shown in Fig. 4a. This direct comparison between the photonic crystal and the slab waveguide shows significant differences in the interference pattern periods. As the interference pattern for the PC waveguide has a longer period, it can be concluded that the wavelength in this waveguide is larger and its effective refractive index smaller as compared to the slab waveguide area. This is consistent with the additional boundary conditions introduced by the periodic hole array. The finding is confirmed in the Fourier analysis of the interference patterns shown in Fig. 4b. To obtain this figure we used a hamming window to terminate the transform and divided the spatial frequency by the sampling length to obtain the depicted spatial period of the interference pattern.

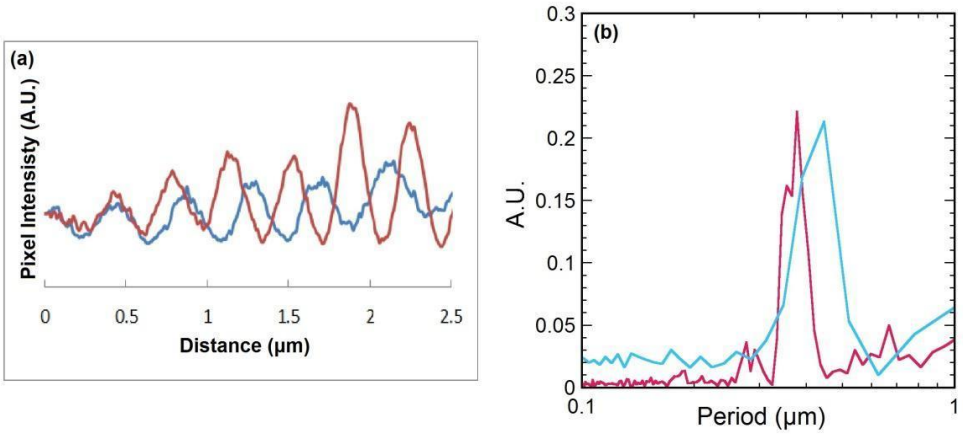

Fig. 4. (a) Line graphs of pixel intensity in the PC defect waveguide (blue) and bulk slab waveguide (red). (b) Periodogram for PC defect waveguide (blue) and bulk slab waveguide (red). The mode in the channel is distinctly shifted toward longer periods.

We used a similar approach for the evaluation of the data obtained in the simulation: Periodograms for the simulation results were determined from time-averaged light intensity distributions shown in Fig. 2b and d. In this case the line graphs were taken at the ITO-vacuum interface for the two waveguides to account for the near-surface photoemission. The comparison between experimental and simulated results for the slab waveguide are shown in Fig. 5. Basic electromagnetic theory predicts that the slab waveguide supports two discrete modes [9 - 11] in the range of λ=390-410nm. These appear in the periodogram labeled 1 and 2. A third mode is near the mode cut-off for the ITO layer and appears in the experimental results only when sampling is taken in the region closest to the in-coupling of light. In the numerical results the penetration depth of this mode is larger and it appears as a prominent peak labeled 3. The difference between the two data sets is thus likely due to a slight over-estimation of the film thickness for the simulation. The peak, labeled 5, corresponds to the beating pattern of the first two fundamental modes. It is clearly seen in the experimental results, but is weaker in the simulation data, probably due to an insufficient sampling length for this very low-frequency mode. Higher order modes corresponding to the frequency-doubled overtones of modes 1 and 2 appear in region 4, but are not clearly discernible in either data set. A more detailed analysis of these planar slab modes may be found in references [6,7].

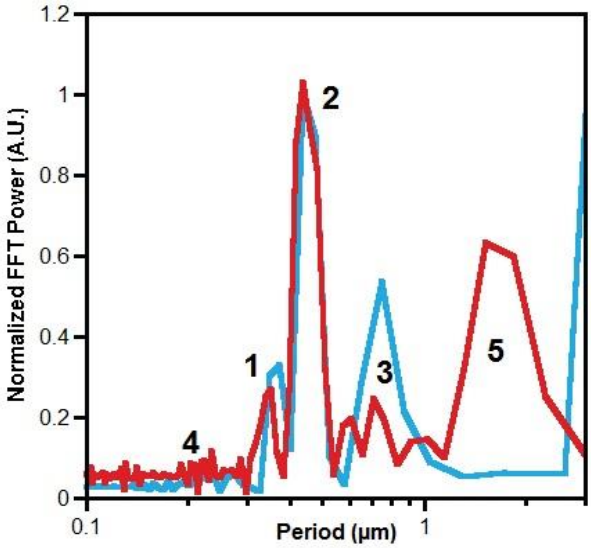

Fig. 5. Periodograms of the slab waveguide for λ=410nm showing experimental (red) and simulation (blue) results for TE polarization. Peaks 1-2 correspond to primary allowed modes. Peak 5 represents the beating pattern of modes 1 and 2. Peak 3 corresponds to a near cutoff mode that appears strongly only in the region closest to the coupling trench.

For the PC waveguide a comparison of simulated and experimental data, is shown in Fig. 6. Here we find the experimental data to be of higher quality than the simulation results, as they show narrower Fourier peaks. The definition of the Fourier peaks depends on the length of the waveguide being considered. In the experiments the length of the PC waveguide is limited by the patterning ability of the FIB, while in the simulation it was limited by computational memory. These limitations have an impact on both cases, but the simulation is more strongly affected and hence its pattern is less well defined and only one major peak is visible in the Fourier spectra. The simulated results show an additional peak at a periodicity of 180nm corresponding to the periodicity of the crystal. This peak is a result of the incident beam coupling at the holes of the photonic crystal lattice. This effect is more pronounced in the simulation due to the small aperture for the input of the electromagnetic field. Furthermore, in the experimental data the coupling efficiency at the holes is likely to be lowered as the hole walls are slightly slanted and the in-coupling is reduced.

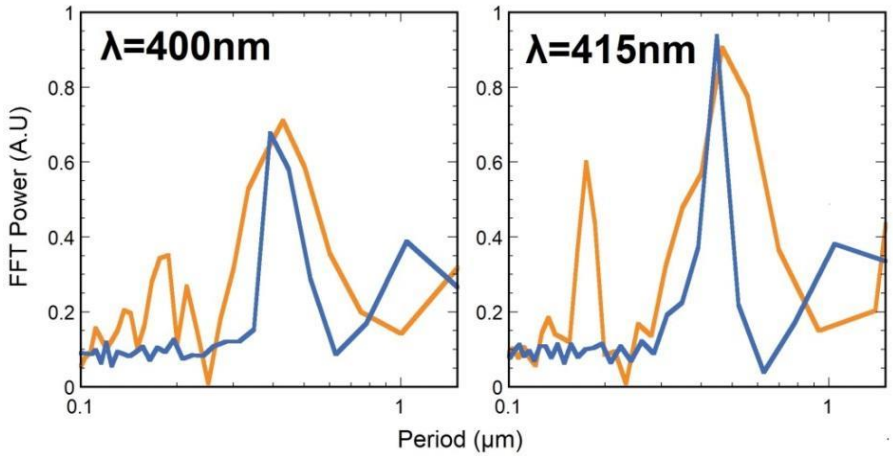

Fig. 6. Periodograms for the interference pattern in the defect channel for experimental (blue) and simulated (orange) data at 400nm and 415nm illumination and TE polarization.

From the Fourier transforms we obtain the wavenumber of the interference pattern, $k_{interference}$. This, along with the known wavenumber of the incident light, allows us to determine the wavenumber of the propagating modes, and thus the effective index, n_{eff}, of the waveguide. For the in-plane components of the wavevectors we have in the current case,

$$\vec{k}_{mode} - \vec{k}_{incident} = \vec{k}_{interference}. \quad (2)$$

$$n_{eff} = k_{mode} \frac{\lambda_0}{2\pi}. \quad (3)$$

By imaging across a range of wavelengths and determining the allowed modes at each frequency we can calculate the wavelength dependence of n_{eff} in the waveguides. In the slab waveguide the effective index of the guided modes decreases in a linear fashion with wavelength as shown in Fig. 7a. The rate of change of the effective index gives the magnitude of the dispersion in the waveguide. The linear decrease follows the predicted dispersion across the measured range for the waveguide geometry and material [8-10]. In the PC waveguide we observe a more rapid change of the effective index for wavelengths in the 390-395nm region as shown in Fig 7b. This indicates strong dispersion for this range of wavelengths.

It is well known that photonic crystal defect modes exhibit extremely large dispersion for wavelengths near the edge of the photonic bandgap [12]. Strong dispersion relates to a low

group velocity and has extensive application in photonic device design [13]. Our results indicate that PEEM may conveniently be used to analyze the dispersion properties in photonic waveguides with photonic crystals holding particular interest. Further work is needed, however, to confirm the mechanism responsible for the enhanced dispersion in our results.

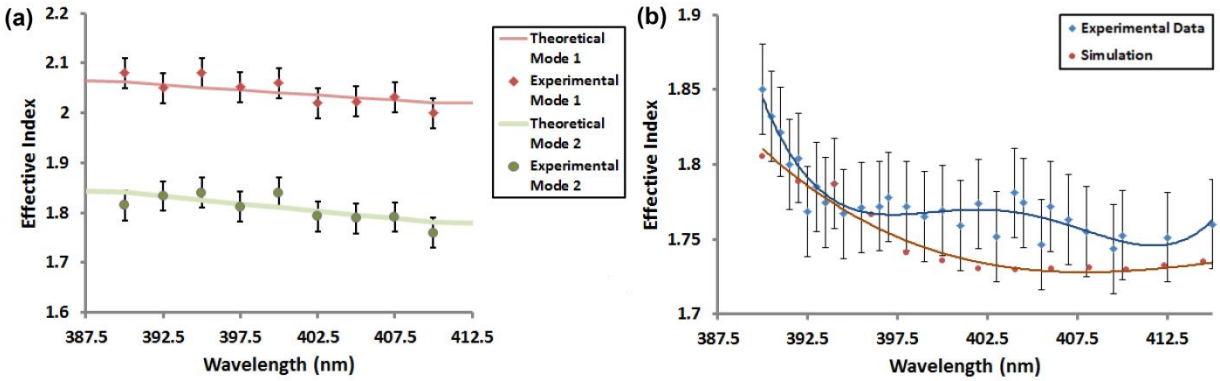

Fig. 7. (a) Theoretical and experimental calculations for the wavelength dependence of the two allowed mode in the slab waveguide. (b) Experimental (blue) and simulated data (red) for the wavelength dependence of the photonic crystal defect mode with polynomial fits to guide the eye.

5. Conclusion

We have applied PEEM to obtain detailed information on wave propagation in planar optical structures. The non-linearity of the photoemission process enhances electric field contrast, allowing efficient spatial interferometry. From the spatial information in PEEM images details on mode propagation, dispersion parameters, and power flow can be obtained which is important for a variety of applications in integrated photonics [14]. We hope to extend our work with PEEM using more comprehensive theoretical models to directly observe slow light and other photonic phenomena.

References

1. R. Könenkamp, R.C. Word, G.F. Rempfer, T. Dixon, L Almaraz and T. Jones, “5.4 nm spatial resolution in biological photoemission electron microscopy” Ultramicroscopy 110, 899 (2010).
2. K. Fukumoto, K Onda, Y. Yamada, T. Matsuki, T. Mukata, S. Tanaka, S. Koshihara, “Femtosecond time-resolved photoemission electron microscopy for spatiotemporal imaging of photogenerated carrier dynamics in semiconductors.” Rev. Sci. Instrum. 85, 083705 (2014).
3. L. Zhang, A Kubo, L. Wang, H. Petek, and T. Seideman, “Imaging of surface plasmon polariton fields excited at a nanometer-scale slit,” Phys. Rev. B 84, 245442 (2011)
4. C. Lemke, T. Leifsner, S. Jaurnik et al. “Mapping surface plasmon polariton propagation via counter-propagating light pulses” Optics Express 20, 12877 (2012)
5. J. P. S. Fitzgerald, R. C. Word, and R. Könenkamp, “ Subwavelength visualization of light in thin film waveguides with photoelectrons,” Phys. Rev. B89, 195129 (2014).
6. J. P. S. Fitzgerald, R. C. Word, S. D. Saliba, and R. Könenkamp, “Photonic near-field imaging in multiphoton photoemission electron microscopy,” Phys. Rev. B87, 205419 (2013).
7. T. Stenmark, R.C. Word, R. Könenkamp, “Determination of the Goos Hanchen shift in dialectric waveguides via photo emission electron microscopy in the visual spectrum” Optics Express 24, 3839 (2016)
8. R. Schlaf, H. Murata, and Z. Kafafi, “Work function measurements on indium tin oxide films,” J. Electron Spectrosc. Relat. Phenom. 120, 149 (2001).
9. A. Yariv, *Optical Electronics* (Saunders College Publishing, Philadelphia, 1991).
10. H. Kogelnik, *Theory of Optical Waveguides in Guided-Wave Optoelectronics*, T. Tamir, ed. (Springer-Verlag, 1988).
11. T. Stenmark, "Photoemission Electron Microscopy for Analysis of Dielectric Structures and the Goos-Hänchen Shift" (2016). *Dissertations and Theses.* Paper 2991.
12. Baba, T. “Slow light in photonic crystals” Nature Photon. 2, 465 (2008).
13. T. F. Krauss. “Slow light in photonic crystal waveguides,” J. Phys. D 40, 2666 (2007).
14. P.K. Tien “Integrated optics and new wave phenomena in optical waveguides,” Rev. Mod. Phys. 49, 361 (1997).

Acknowledgement

This research was supported partly by the US-DOE Basic Science Office under Contract No. DE-FG02-10ER46406.